Production Engineering
https://doi.org/10.1007/s11740-023-01233-3

PROCESSES

A novel process chain for the automated repair of leading edges in aircraft engines

Robert Kenneweg[1] · Klaas Maximilian Heide[1] · Volker Böß[1] · Berend Denkena[1] · Hans-Henrik Westermann[2]

Received: 27 July 2023 / Accepted: 16 October 2023

Abstract
Due to impacts and constant stress, the leading edges of aircraft engine blades often lose their shape, while the other parts of the blade are still functional. This results in unnecessary performance losses. Currently, there is no method for a fast and effective repair process as the initial shape of the blade cannot be restored. This paper presents an automated re-contouring process chain for leading edges without prior material application. Thus, it is a sustainable approach to extend the lifespan until an energy-consuming welding process can be performed. It consists of an in-machine scanning process to obtain information about the worn shape, a subsequent target model generation based on the worn shape, and an automated process planning. The process chain is evaluated using a universal, leading edge workpiece. The results show that the target requirements for shape and smoothness are fulfilled.

Keywords Maintenance · Manufacturing system · Adaptive manufacturing · Automation · In-process measurement · Sensor

1 Introduction

Besides other major components of an aircraft, like the fuselage and the wing, the engine represents one of the most complex and expensive single components. Figure 1 gives a schematic overview of a modern aircraft engine and shows the large number of blades.

The function of the engine is to provide the thrust to move the aircraft forward. In addition, electrical, hydraulic, and pneumatic power must also be supplied to operate instruments and move other devices, such as the landing gear and flight control surfaces [2].

According to a forecast by Airbus, around 39,000 new aircraft are needed in the next 20 years. Around 40% of these aircraft are replacements for passenger planes and the remaining 60% are due to air traffic growth. Thus, the total number of aircraft required totals about $ 4.9 trillion [3].

✉ Klaas Maximilian Heide
heide@ifw.uni-hannover.de

[1] Institute of Production Engineering and Machine Tools, Leibniz University Hannover, An der Universität 2, 30823 Garbsen, Germany

[2] MTU Maintenance Hannover GmbH, Münchner Straße 31, 30855 Langenhagen, Germany

While the global engine Maintenance, Repair, and Overhaul (MRO) revenue is, due to the coronavirus, estimated to be around $30 billion in 2021, it is also expected to increase rapidly by about 75% to approximately $52 billion by 2026 [4]. A further, albeit smaller, increase is also expected in subsequent years, with a total volume of more than $56 billion targeted for 2031. This expected growth leads to increasing challenges for companies regarding the capacity and efficiency of MRO processes. These challenges can be met by several organizational measures, e.g., an increase in production capacities or expansion of the shift operation. Besides these structural adjustments, innovative MRO processes are needed for automation and corresponding efficiency improvement [5].

During operation, rotor blades are exposed to various wear mechanisms resulting from operating conditions and design features of a turbofan engine. Typical wear mechanisms on rotor blades include abrasion, erosion, corrosion, and contamination. Abrasion describes the damage that occurs in the blade tip area caused by dynamic rubbing against the turbine casing. In the case of newly manufactured engines, this is deliberate since an optimum gap is set between the rotor blade and the housing during the initial run-in. In further operation, however, unwanted abrasion can also occur, for example, when maneuvering and flight loads

Published online: 29 January 2024

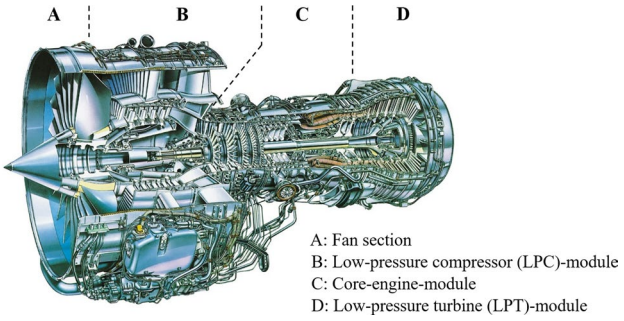

Fig. 1 Process characteristics leading edge re-contouring [1]

cause elastic bending of the rotor shaft, which in turn, causes the blades to rub against the turbine housing unintentionally.

Erosion includes the tribological removal of material from the blades through interaction with sucked-in foreign bodies, such as sand, dust, volcanic ash, ice, small stones, and metal parts, as well as birds. Particularly during takeoff and landing, as well as during ground-based operations in general, foreign bodies are sucked in by the engine. These hit the rotor blades at high relative velocity. The impact can cause material removal from the blade. Corrosion can occur as a result of flowing corrosive media and describes a chemical damage process to the blade material. Industrial exhaust gases, as well as salty sea air, are typical corrosive media. Special fuel components and their combustion products can also have a corrosive effect. Contamination occurs in the form of permanent deposits of dirt particles on the blades. In this case, the deposit generally occurs over the entire component, with special component areas, such as the blade root transition or the cooling air holes, being particularly susceptible. The deposited dirt particles make for a rougher surface, thus having a strongly negative effect on the flow boundary layer and the mass flow rate. The wear mechanisms are also generally superimposed by manufacturing scatter and, possibly, previous repairs of the components. [6, 7]

Given the various locking mechanisms in the operation of moving blades with simultaneously expected long service life, the maintenance of the blades plays an important role [7]. At regular intervals and after special events, e.g., a bird strike, moving blades are inspected and individually repaired depending on the degree of damage. Meanwhile, the blades are inspected for unacceptable damage, deformation, or cracks and, if necessary, discarded if the detected damage is irreparable.

Of particular interest to the present publication are the maintenance procedures for re-contouring the leading edge geometry of moving blades. As shown in Fig. 2, re-contouring attempts to restore the nominal geometric properties of the moving blade as best as possible by a defined removal of material at the leading edge. The left part of Fig. 2 shows an example of the deviation between the nominal contour and the contour before the repair. The right part shows the deviation between the nominal contour and the contour after the repair.

How a rotor blade is to be repaired and the manufacturing processes that can be used depends on the design and construction of the blade. Corresponding information is provided in the respective engine manual of the manufacturer. Yet, usually, only the rough process sequence of maintenance and component-related boundary conditions of the repair are specified. The specific manufacturing process for repair is usually not specified. As long as the prescribed requirements are met, any suitable repair process can be used. Various concepts are known from industrial practice, whereby manual grinding with a belt grinder, including subsequent polishing steps, is usually used. This direct processing of the blades requires much skill, a lot of experience, and focuses on re-contouring a leading edge that has been blunted by operation, for example, by grinding the flanks. Repairable damage caused by foreign body impacts is also blended with smooth transitions during the hand-guided grinding process. In all work steps, the focus is on minimizing material removal and ensuring high contour accuracy per the manufacturer's specifications. In addition to conventional manual grinding, other processes are used for re-contouring the leading edge geometry with the aid of laser beams [9, 10], the use of radius grinding tools or contour cutters in contour-adapted hand-guided fixtures [11], and machine-guided brush chip removal [12].

The importance of high re-contouring quality arises from the fact that important performance-leading aerodynamic parameters are directly linked to a change in leading edge geometry. Figure 3 shows an example of the relationships based on the pressure distribution in a CFD

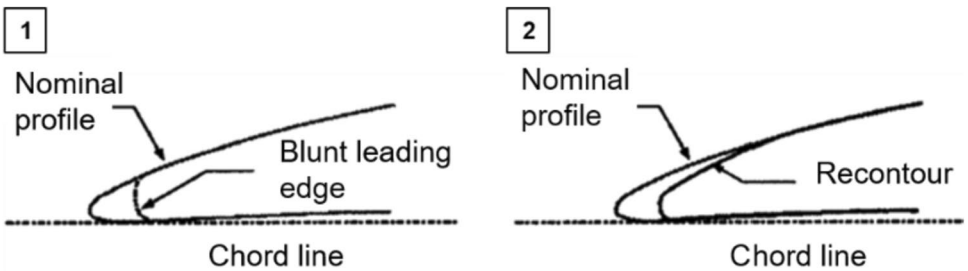

Fig. 2 Process characteristics leading edge re-contouring [8]

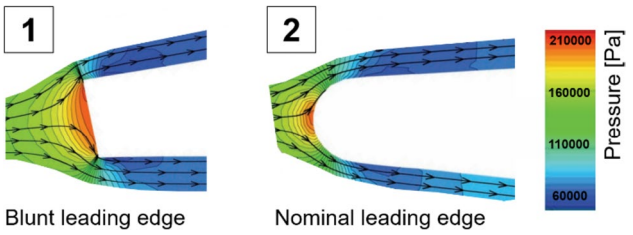

Fig. 3 Flow around leading edge for a blade with a blunt leading edge (1) and a blade with a nominal leading edge (2), based on [13]

simulation of different leading edge geometries of guide vanes:

The investigations show that even small geometric changes in the nominal leading edge lead to numerically verifiable effects that harm efficiency as well as fuel consumption, thus also directly on the resulting CO_2 emissions. The need to drastically reduce CO_2 emissions to limit global warming affects the aviation industry both in terms of public perception, associated with demands for more efficient engines and lower CO_2 emissions per passenger kilometre, and directly financially via CO_2 pricing under the EU Emissions Trading System (ETS) [14]. The overarching goal of high-performance and efficient aviation, which is linked to this initial situation, includes not only the operation of aircraft but also their maintenance [15]. Automated precise and repeatable re-contouring of the leading edge not only offsets the negative effects, but also achieves material, time, and resource efficiency gains through longer use of the components, which in turn, have a positive impact on the degree of utilization of the engines.

As shown, the leading edge has a high impact on the efficiency of the engine. However, an essential factor for substantial improvements is the holistic consideration of the process chain [16]. In the build-up welding repair process chain for turbine blades, milling is a central step in which the basis for dimensional accuracy is established before final grinding. Companies have already demonstrated the potential of geometrically adaptive NC paths based on initial measurements of the actual geometry [17].

In the re-contouring of leading edges, different challenges can be identified in terms of production technology resulting from the characteristics of the machining task, for example, thin-walled components, mostly difficult-to-machine materials, and spatially geometric tool paths for the generation of free-form surfaces. The highest requirements are set for the milling of engine blades made of high-temperature superalloys and titanium aluminides, which are chosen due to the high component loads in aircraft engines [18]. In particular, there is the definition of suitable machining strategies and process-reliable cutting parameters. In principle, the production of leading edges on engine blades is generally divided into roughing and finishing operations. In roughing, the part is machined with a high metal removal rate and followed by a finishing operation with low machining overheads to finalize the workpiece. The machining strategy for re-contouring a leading edge represents a finishing operation due to small material removal rates and low stepover distances. Especially in the case of machining titanium alloys, elastic deformations have a negative influence on the manufacturing result [19]. Moreover, very thin leading edge areas are sensitive to elastic deformations during the milling process. If down milling is used for machining, the chip thickness is zero millimeters at the entry of the cutting edge into the workpiece. In addition, chip thickness increases along the cutting path with increasing tool engagement. Therefore, the chip thickness is below the minimum chip thickness during a long cutting path from the start of the engagement. Instead of separating material removal, material displacement with systematic scraping occurs. Therefore, a long friction phase appears, and the chip thickness is maximized at the moment of the cutting-edge exit. In up-milling, the maximum chip thickness is achieved at the point where the cutting edge enters and decreases to zero along the cutting path until the cutting edge exits the workpiece. Thereby, the cutting chips are only minimally attached to the cutting edge and are wiped off at the latest during the re-entry of the cutting edge into the workpiece. In combination with the previously described effects, higher surface finishes and more stable process control are achieved when up-milling is used [20, 21]. Therefore, up-milling is preferable to down-milling for the re-contouring of leading edges on engine blades, whereby spherical-head end mills are used for the production of free-form surfaces in the re-contouring of leading edges. Technically, the tool center is a critical point when using spherical-head end mills because the cutting speed at this point tends to be zero. At the same time, chip removal is problematic due to the small chip space at the tooltip. By adjusting the spindle axis in the range of $\varkappa = 10° - 15°$ regarding the workpiece surface, the contact zone is shifted out of this range, and a higher minimum cutting speed, as well as improved chip formation, is achieved. Preliminary experiments showed that the most stable process dynamics, including the highest surface quality, were obtained during finishing with the equal value for cutting width a_e and tooth feed f_z, $f_z = a_e$. For the evaluated cases with $a_e > f_z$, a higher chatter tendency in correlation with larger roughness depths could be observed. Process characteristics are shown in Fig. 4.

In regards to the overall repair of blades, there are several specialized works. Some researchers investigate how to perform repairs on more damaged blades. This involves a complex process of adding material through a laser welding process and then using different methods to restore the original nominal shape [22–26]. Further research is investigating

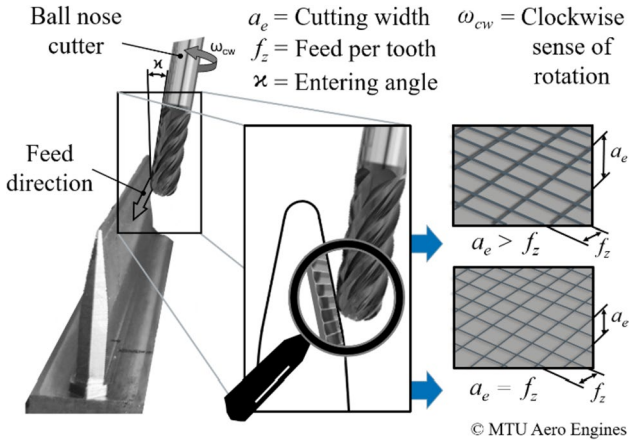

Fig. 4 Process characteristics during leading edge re-contouring

the adaptation of the defective areas to the remaining part of the blades. In most cases, this is done by interpolation or extrapolation of the non-defective areas, which ensures smooth transitions but runs the risk that the shape achieved does not meet the initial requirements [27, 28]. Nearly all studies use shape recording methods, but often, these are manual. For the described methods, the generated point clouds have to be reconstructed into curves or surfaces, for which some algorithms are described [29, 30].

The works described require the application of material to restore the initially planned shape as accurately as possible. Only the transition to the other areas is adjusted. In addition, none of the work describes an overall and generally usable and low-energy method of restoring engine blades to extend their life span. As described, the leading edges have a high influence on the engine efficiency and, at the same time, are subjected to high loads, which results in severe wear. Thus, a novel, holistic approach for the re-contouring of leading edges was developed. In order to delay an energy- and time-consuming material application as long as possible, while still fulfilling the requirements, the described method uses the initial target model and adapts it to an automatically recorded point cloud. The presented method is, therefore, a link between new part production and welding repair (see Fig. 5). For this, the novel process chain consists of three automated main steps:

(1) Shape acquisition of the worn blade (scanning process).
(2) Generation of an adapted model, and.
(3) Process planning.

It is described and investigated in the following sections. In the end, a critical evaluation of the results is conducted, and future tasks are identified.

2 Determination of the worn shape

The leading edges of engine components are subjected to very high thermal and mechanical loads during service. As a result, various wear types and deformations occur on the leading edge over a certain period. These defects must be localized and transmitted to an automated remanufacturing process in the format of geometric data. State-of-the-art measurement methods and concepts have deficiencies in automation while maintaining high accuracy. Currently, manual and complex pre- and post-processing steps are still necessary to initialize an error-free recondition process based on the measured data. As part of the reconditioning, this paper introduces an innovative and fully automated scan concept to determine the worn shape of the workpiece. This can be achieved by a laser line scanner integrated into a CNC machine and a self-developed software framework.

In this research work, a DMG HSC 55 linear milling machine with a Heidenhain iTNC 530 control is used as a

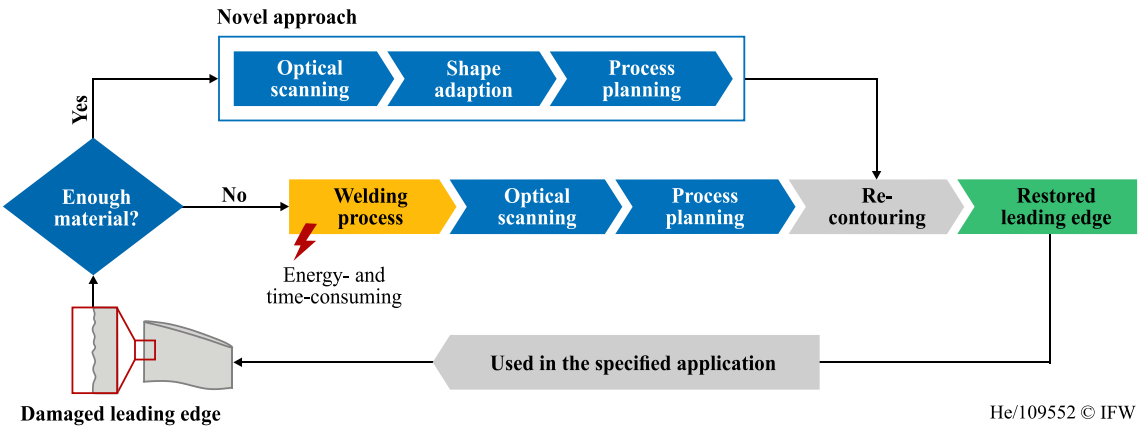

Fig. 5 Integration of the novel approach in leading edge restoration

5-axis CNC machining and scanning center. For this purpose, the HSC55 is extended with an industrial PC by Beckhoff and an optical laser line sensor LJ-V7080 by Keyence. The LJ-V7080 works with the triangulation principle and consists mainly of semiconductor lasers, lenses, processors, and a CMOS chip. The emitted optical laser beam is expanded to a laser line on the target object. The resulting reflection on the object is processed by the CMOS chip. With this measuring principle, height profiles can be determined quickly and precisely in two dimensions. By using a motion axis, the 2D sensor line profiles can be extended to a three-dimensional point cloud. The point cloud can be converted into a face or solid body with the support of CAD or mesh software.

Table 1 shows the specifications of the Keyence LJ-V7080 optical laser line scanner [31]. The LJ-V7080 uses a blue semiconductor laser (class 2) with a wavelength of 405 nm as the light source. The point data resolution along the laser line is 50 µm. By using the high-speed mode and reducing the laser linewidth, the maximum trigger interval is 64 kHz (16 µs).

The manufacturer Keyence specifies the measuring accuracy in height (z-axis) as linearity related to the measuring range under laboratory conditions. In order to evaluate the applicability of the laser line sensor according to the specified accuracy requirements, a measurement test was performed in the CNC machine tool on a measurement sample part made of steel. It was measured tactilely on a coordinate measuring machine Leitz Reference XI 10 · 7 · 6 / B5 and scanned with the LJ-V7080 sensor in the CNC machine tool. As a result, measurement accuracy of about 10 µm (in the range of ± 5 mm to the reference line) and up to an average of 30 µm (range end) was detected for the Keyence LJ-V7080. Consequently, the sensor reference distance should be set in sensor path planning for measurement tasks with high requirements.

Table 1 Specification of laser line sensor LJ-V 7080

Property	Value
Type	Blue semiconductor laser
Wavelength	405 nm (visible beam)
Reference distance	80 mm
Spot size (reference distance)	Approx. 48 mm × 48 µm
Measuring range (high, z-axis)	± 23 mm (46 mm)
Measuring range (width, x-axis)	
Top (near side)	25 mm
Middle (reference distance)	32 mm
Buttom (far side)	39 mm
Profile data interval (width)	50 µm (800 pixel)
Sampling cycle (high speed mode)	Max. 16 µs (64 kHz)
Linearity z-axis (height)	± 0.1% of measuring range
Repeatability (high, z-axis)	0.5 µm
Repeatability (width, x-axis)	10 µm

For a fully automatic measuring and scanning system, fast and error-free communication between various hardware components and software is essential. In the introduced scanning setup, the control unit of the optical sensor and machine control is connected to an industrial PC (Ethernet, Profibus, and USB). In addition, a self-developed scan software, including its data structure, is created and implemented on the interconnected industrial PC system. The software processes and merges the data of the different hardware interfaces during the scanning process to generate a 3D point cloud.

Figure 6 illustrates the structure of the scanning methodology. The scanning process begins with a clamped workpiece in the CNC machine tool. In the first process step, a hybrid measuring-scanning program is individually created for the workpiece. This is performed by cross-linking to the Siemens NX CAM module via the NX Open programming interface. By loading idealized CAD-model data and a self-generated surface recognition and path planning algorithm, collision-free sensor paths adapted to the workpiece surfaces are generated. In this context, the sensor position in the working machine area and the reference distance of the laser line sensor will be observed. The generation of sensor paths is realized based on the standard NX path planning cycles, which were originally designed for milling operations. The generated tactile probing paths and calculated scanning paths are compiled into machine-specific NC-code and directly transmitted to the CNC machine control by the scanning software.

At the beginning of each measuring task, the clamped part is referenced and oriented in a workpiece coordinate system by a standard tactile 3D touch probe. Afterward, the scanning process starts. To obtain an optimum incident angle of the laser line on the leading edge, a 3-axis and a 3 + 2-axis sensor path strategy are pursued during the scan process. During the scan process, the axis data of the machine tool and the sensor measurement line are read out and cross-linked. The motion speed of the laser line sensor head in the CNC machine is limited according to the sampling frequency (changing data value) of the hardware components and the computing speed of the software application. Currently, the software timer algorithm, which is implemented in a Windows form application, is the slowest section. A calculation speed of approx. 20 ms (50 Hz) is experimentally determined. The sensor profile line can be read out with a frequency of about 666 Hz (2 ms, via USB), and the axis data from the machine control with approx. 125 Hz (8 ms, via Ethernet).

For a structured and manageable point cloud, the scan and axis data are buffered in a definable constant request interval during the measurement task. A fully automatic activation,

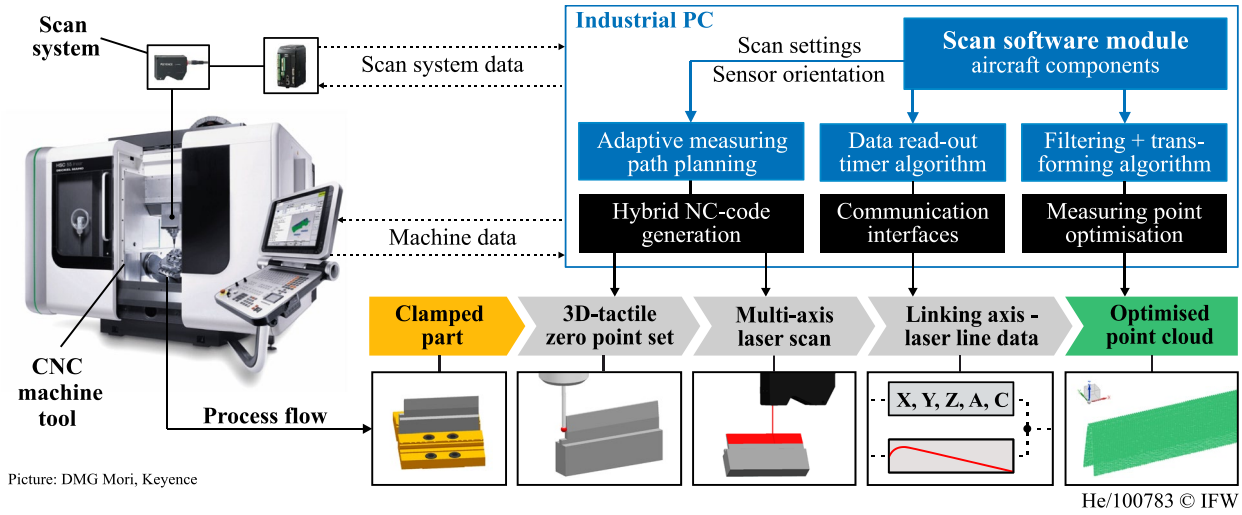

Fig. 6 Fully automated scanning methodology

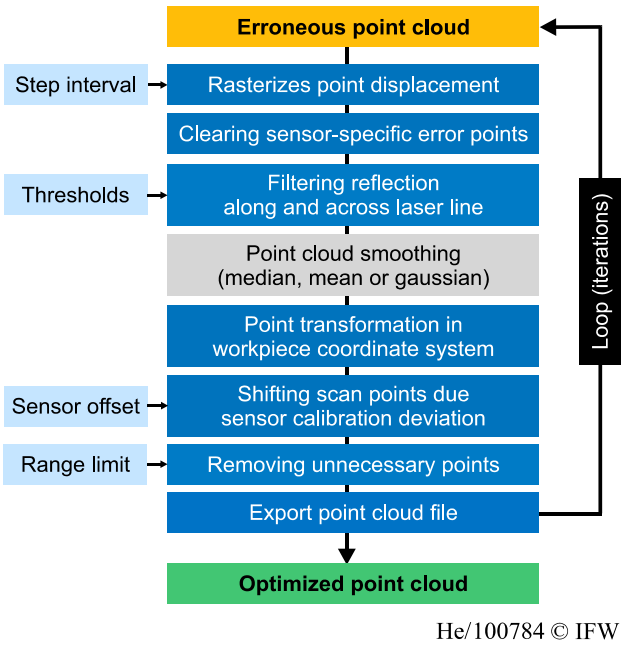

Fig. 7 Algorithm for filtering and transforming scan data

pausing, and stopping of the measuring system, as well as saving of the point, will be performed by moving the machine axis to defined reference positions. Therefore, no external input during the whole process chain is necessary.

To achieve an optimized point cloud for each measurement task, an algorithm for processing the scan data was developed and implemented in the scan software module (see Fig. 7). The algorithm rasterizes the recorded measuring points (displacement due to time delay), clears sensor-specific error points (Keyence error code), and removes reflections (over-height measuring points). In addition, multi-axis scanned measuring points are transformed into the workpiece coordinate system. Scan points are shifted if the sensor head is inaccurately calibrated and the measuring range is restricted to remove unnecessary elements in the point cloud, e.g., the clamping system. Optionally, the recorded points can be smoothed with a median, mean, or Gaussian filter.

The data processing algorithm starts based on the stored point cloud (raw data) after the scanning process is finished. This avoids unnecessary delays during the scanning process and allows additional filtering with modified settings. The raw data of the scanning operation and the related selected sensor settings is stored as a clear word text file (.txt) in a folder structure and file container. Therefore, the scan data can be archived locally, on a network drive, or in cloud storage. Each measuring point is contained in the data as X, Y, and Z coordinates in the process-defined workpiece coordinate system. In addition, for each measuring point, the angles of the A and C axis of the milling machine, the measuring line as a number, the scanned area as a value, and the Keyence-specific measured value or error code are appended to the data structure. A simplified point cloud in X, Y, and Z format can also be stored.

In the first process step of the measurement data processing algorithm, the recorded measuring points are rasterized. In the scan process, sensor and axis data are requested at a defined interval (overrun defined axis positions on the movement axis) and temporarily stored in an array. Due to the sampling frequency and axis movement speed, an offset occurs between the target and the stored real axis position. The deviation depends on the feed rate of the axes and the calculation speed of the software, which varies on a Windows system. In the algorithm, the recorded positions on the motion axis are rounded to a fixed value, e.g., to the nominal

dimension. Thereby, a uniform point grid is created in the point cloud. After rasterization, invalid measurement data points are removed by the algorithm. Invalid data points are measurement points that are not recognized by the optical laser scanner. The Keyence control unit outputs an error code instead of the actual measuring point. In the third step, over-high measurement points resulting from reflections are eliminated. Based on a defined threshold value, the z-axis direction of the measured points along the laser line and in the direction of the scan movement are checked in pairs. If the threshold value is exceeded in positive and negative z-axis direction $\Delta h > h_{threshold}$, the respective measuring point is identified as a reflection point and will be deleted (see Fig. 8).

If the point cloud is too noisy, the measurement points can be smoothed by the algorithm. For this purpose, 3 × 3 matrices are set up step-by-step over the point cloud grid, and a mean, median, or Gaussian filter can be applied. After all error points have been removed or smoothed, the measurement points are transformed into the workpiece coordinate system. This is done based on the recorded and stored axis positions (A- and C-axis) for each measuring point through calculation by the rotation matrix. If the scanning system is not precisely oriented in the machining area, there will be an offset between the multi-axis scans. This can be corrected with the aid of a manually specified position. Therefore, an optimally calibrated sensor is currently required for fully automated data processing. In the last step, the measurement area is restricted based on the transformed and aligned point cloud. By using a bounding box with minimum and maximum X, Y, and Z values in the workpiece coordinate system, unwanted areas, such as the scan of the clamping system or unnecessary workpiece areas, are removed. This also reduces the size of the point cloud. After one cycle of data processing, an optimized point cloud is available for further processing. It is also possible to refine the point cloud through further iterations.

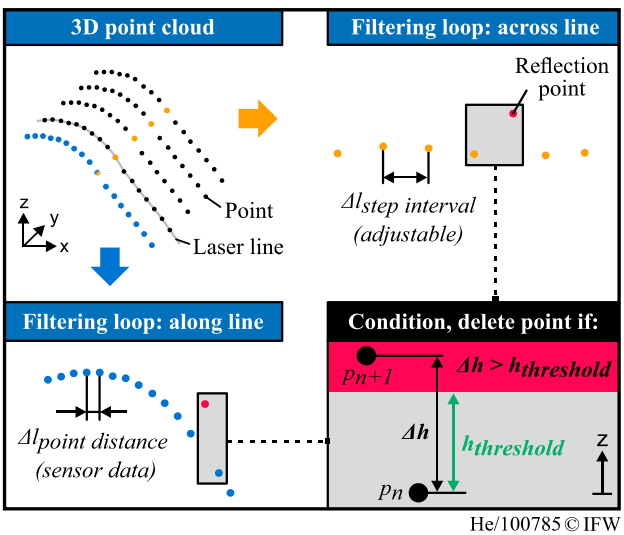

Fig. 8 Filtering of reflection along and across laser line by threshold

3 Target model adaption

Based on the acquired point cloud of the actual shape of the leading edge, a new target model for the tool path generation must be defined. For this, the CAD-model that describes the originally planned nominal shape of the workpiece is adapted to the point cloud in order to reduce the material removal and ensure a smooth transition between the machined and unmachined area of the repaired blade.

In the first step, the CAD-model is prepared, as shown in Fig. 9. This step must be done once for every part design. Initially, the models are reduced. For this, the faces of the volume are extracted. The resulting surface model is evaluated manually, and unnecessary surfaces that do not influence the leading edge are removed. From the remaining surfaces, the areas relevant to the fitting are extracted. The number of remaining surfaces and their complexity influence the speed of the later-performed adaptation process to a great extent. Therefore, the reduction leads to considerable speed advantages. After this step, only three surfaces remain; the circular segment ("radius"), which represents the edge itself,

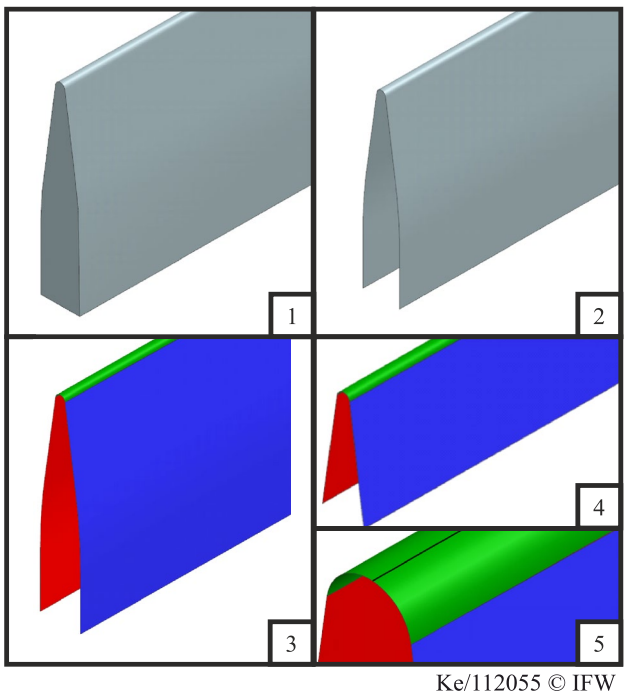

Fig. 9 Preparation of the CAD-model. Volume model (1), reduced face model (2), divided face model (3), trimmed face model (4) and directional curve (5)

and the two flanks, which are the beginning of the suction and pressure side. In addition, a so-called directional curve must be created to create two-dimensional curves. The directional curve runs over the maximal turning points of the individual profile sections (see Fig. 9, Detail 5). Since these points are difficult to describe for automation, this curve is also initially created manually. Even though preparation requires some manual steps, it is not an obstacle to automation since preparation must only be performed once per workpiece design. All blank-dependent steps remain automated to a higher degree.

Since leading edges have a similar cross-section along the directional curve, two-dimensional sectional curves, independent of the complexity of the face, can be used and adjusted for the model adaption. For this, the reduced model is automatically cut with planes. The planes are distributed equidistantly along the directional curve and are aligned so that the plane normal always corresponds to the tangent of the directional curve at the intersection with the plane. Each created plane is intersected with the surfaces of the reduced model, resulting in three intersection curves. To reduce computing time, as most calculations only consider coordinate, and to keep the process algorithms more comprehensible, each section is aligned with the X-Z-plane. For this purpose, the direction of the plane normal of the examined section is oriented to the Y-axis and moved to the origin via a translation vector and two rotation matrices. Using the translation vector, the plane is shifted towards the origin of the coordinate system. Looking at any sectional plane, it can be aligned with the axes of the coordinate system via two rotations. Then, the curve must be oriented within the plane. For this purpose, the normal of the intersection curve at the point of intersection with the direction curve is used. The same point is moved to the zero point, and the normal vector is aligned to the Z-axis of the underlying coordinate system via an additional rotation matrix. Afterward, the point cloud is adjusted using the same translational vectors and rotation matrices, as described in the following. As the scanning process is adjusted to the intersection planes, every point is assigned to one cutting plane. Therefore, a projection onto the plane, as described in [32], is not necessary. To create an adapted shape of the blade with small differences from the worn shape, the intersection curves must be fitted to the point cloud in an iterative process. Due to the high mechanical stress of the blades, the location of the point cloud and the intersection curves in each section can differ to a great extent. Therefore, the intersection curves are moved in the X-direction until the minimum and maximum X-values of the curve are in the middle of the equivalent values of the point cloud (see Fig. 10, Part 1).

After the preparation of the model and the point cloud, the adaption process itself begins. This process can be divided into two main adaption methods: rigid and flexible

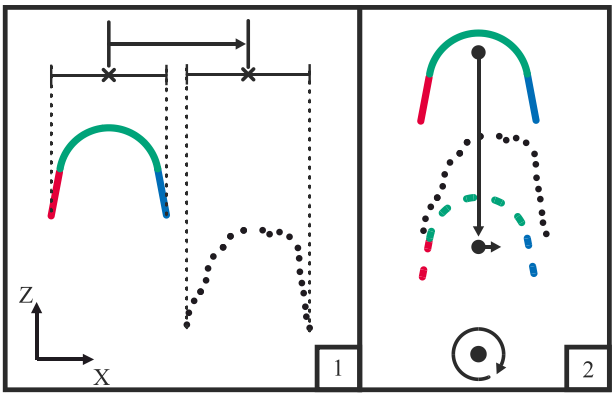

Fig. 10 Pre-adaption (1) and the rigid adaption process (2)

adaption. The rigid adaption does not deform the intersection curve, it only aligns the radius that is optimized and centred in the point cloud. In contrast, the flexible adaption deforms the flanks of the intersection curve for a smooth transition between the machined and unmachined area on the repaired blade. First, a rigid transformation of each intersection curve is conducted along the Z-axis (see Fig. 10, Part 2). For this, a straight line is built through each assigned point. Afterward, the Z-value of the length from the intersection point between the intersection curve of the radius and the assigned point is calculated. Because the machining process only subtracts material, the new target model must be inside the actual contour. Therefore, the smallest value is used for the first rigid transformation. If this requirement is fulfilled, the model is moved as close as possible to the point cloud to minimize material removal. In this case, only the radius is considered because it must not be deformed and must, therefore, lie completely within the model. After the first Z-adaption, a translation in the X-direction is conducted. While the smallest value was used for the first shift, this transformation focuses on a central alignment. For this, straight lines are laid through each assigned point, but this time in the X-direction. Again, only the radius curve is investigated. In most cases, there will be two points of intersection with the radius curve. To assign the point to the proper point of intersection, a middle line is created from the direction curve pointing in the Z-direction. Afterward, the distance between the point of the point cloud and the point of intersection that lay on the same side is calculated. This distance is calculated for each assigned point of the point cloud. Afterward, the smallest distance for each side is determined. Because it is ensured that the radius lies completely inside the point cloud, the left distance is then multiplied by -1. With these two values, the arithmetic mean is calculated and used as the length of a translation vector in the X-direction. All three intersection curves are then translated using this vector. The Z-adaption and X-adaption are repeated until the resulting

translation distance is smaller than 0.01 mm or the number of iterations exceeds 20.

After fitting the target radius, the flanks are adapted flexibly to the point cloud. For this, the flank curves are described as b-spline curves. This type of spline is based on basic functions of definable degree, which overlap in the individual areas of the curve. The main parameters that define b-spline curves are pole points, node vectors, and the degree of the polynomial. Pole points directly influence the deformation of the curve by drawing the curve in the direction of the respective pole points at a specific point of the curve. The node vector is a monotonically increasing sequence of numbers that describes the areas of the curve in which the individual polynomials are not zero, i.e., influence the shape of the curve. The first and last elements represent the bounding parameters of the curve. The number of elements in the node vector is defined by adding degree n, the number of pole points p, and one. In addition, the node vector can be used to determine the area of influence and the point with the greatest influence on the individual pole points.

The flexible adaptation is based on an adapted shift of pole points and the addition of pole points at specific parts of the curve (e.g., parts with the highest distance to the point cloud). At the beginning of the flexible adaption of the flanks, the distance between the points of the point cloud and the intersection line is calculated using the same method as the rigid X-direction translation. Each point of the point cloud is assigned to the point of the curve where the line in the X-direction intersects. Additionally, each curve is analyzed regarding the number of pole points and the degree. If the number of pole points comes below a value that can be defined beforehand, poles are added to the curve. To ensure that a pole point is added at the intended spot, a knot value is added to the vector n-times. With this, n poles are added, with one being at the spot of maximum distance. Pre-existing pole points are altered in the process.

Afterward, for each pole point, a translation vector is calculated the following way (see Fig. 11, Part 1): The average value of all distance values d_p of the points that belong to the influence area of the pole point is determined. Due to the elastic pull of pole points, the average reduces the distance between the point cloud and curve, while a translation out of the point cloud is unlikely, considering the expected shape. Then, the distance d_r between the projected point with the greatest influence and the beginning of the radius is calculated. The value is normalized to a selectable length that describes the length of the transition between the machined and unmachined parts of the blade. Values larger than 1 are altered to 1. The value is multiplied by the initial length of the translation vector to obtain the adapted length. Similar to the X-alignment, the direction of the vector is along the X-axis. The length adaption ensures a smooth transition is created between the radius and the unmachined area. Like

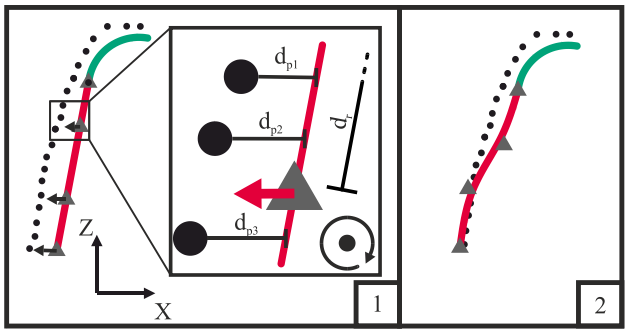

Fig. 11 Translation vector calculation (1) and the resulting adaption (2)

the rigid transformation, the flexible transformation of the flanks is an iterative process. After the final iteration, the second pole point next to the radius is aligned with the first pole point and the second pole point of the radius to improve the smoothness. This procedure ensures a tangential transition between the curves (see Fig. 11, Part 2).

Finally, the adapted curves are used for an automated surface reconstruction using the application programming interface NX Open. For this, four additional curves are created that connect the cross sections; two curves at the end of the flank curves and one curve each at the beginning and the end of the radius. These curves result in a mesh that can be filled to obtain an adapted surface model. Based on this model, a manually planned initial process planning is adapted. This process planning includes used tools, milling strategies, process parameters, and tool path. Using the adapted model, the tool path is modified accordingly, and an NC-code is generated.

4 Experimental evaluation

To ensure that the described methods lead to a repaired shape that fulfills the targeted repair requirements, a test shape was developed (see Fig. 12). The initial basis for the design of experimental parts were workpieces with basic dimensions of 110×45×5 mm. From this, eroded surfaces and a leading edge with uneven removal were simulated for the worn model. Six sections were made over the length of 110 mm by varying the radii (R) and distances (S). The design was focused on an eroded surface represented by a strongly flattened appearance. The initial target model is based on a fictional repair manual and is designed using only four sections. As it represents the new workpiece and the worn model is created by simulated material removal, the initial model encloses the worn model completely and has a rounded edge, which allows good separation of the airflow.

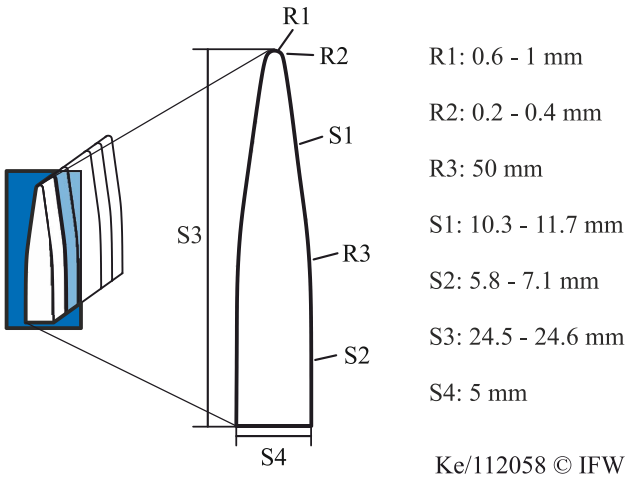

Fig. 12 Design and values for the reference work piece

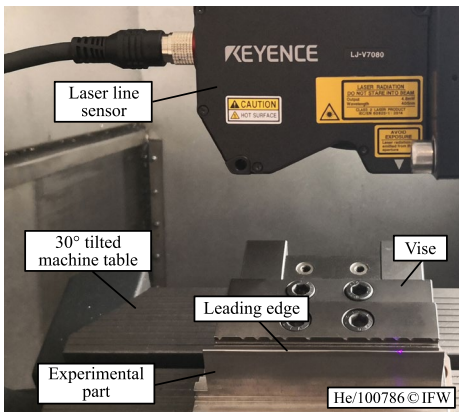

Fig. 13 Automated 3 + 2-axis laser line scan in DMG HSC 55

Based on the CAD-model, experimental parts were machined on two different 5-axis machining centers, a DMU 125 monoBLOCK, and a DMG HSC55 linear. Afterward, the leading edges were scanned with a 3 and 3 + 2 multi-axis scan method (see Fig. 13), which is presented in Sect. 2. During the scanning process, it was observed that the optical laser line system tends to mismeasure strongly curved surfaces and edges due to the variable and oblique angle of impact. These are recognizable in the laser profile line data in the form of deviating measuring points. Furthermore, metallic surfaces reveal a reflective behavior, which also complicates the scanning process. To measure the worn shape of the leading edge with high precision and point density without any manual pre-treatment, sensor and scan settings are experimentally investigated. The sensor and scan process settings that lead to satisfying measuring results are shown in Tables 2 and 3. It is to be highlighted that the samples are scanned without an affixed anti-reflective spray.

Table 2 Sensor settings

Properties	Value
Sampling frequency	1 kHz
Parallel Imaging	Disabled
CMOS sensitivity	High dynamic range 3
Exposure time	960 µs
Imaging mode	Standard
Light intensity	2 times
Synthesis	3 times
Peak detection sensitivity	4
Peak selection	Standard
Peak width filter	Off
Deadzone Process	disable
Median x-axis	Off
Smoothing	1

Table 3 Scan process settings

Properties	Value
Feed rate	50 mm/min
Motion axis	X
Measuring axis	Z
Scan step interval	0.5 mm
Scan strategies	3- and 3 + 2- axis
Scan reference level	Sensor reference distance
Measuring width	30 mm
Number of scan paths	1 per surface

After scanning, the filter algorithm presented in Fig. 7 (Sect. 2) was conducted to remove reflections and transfer the multi-axis 3 + 2 scans to the workpiece coordinate system. A threshold value of 0.2 mm (0.4 mm, 3 + 2 axis scan data) was set as the threshold value for the reflection filter to remove error points across and along the laser scan line. The transition between 3-axis scans and 3 + 2-axis scans was trimmed with the bounding box method to eliminate duplicate measurement points. Thus, the measurement errors at the edge area, which lead to imprecise points due to the inappropriate angle of incidence of the laser on the surface, were also removed from the point cloud. A gap < 0.5 mm between the three single scans was tolerated.

Figure 14 shows the generated, error-free point cloud of a scanned leading edge.

To qualify the measurement accuracy of the introduced scanning method, an experimental part was measured with the scanning system in the CNC machine and tactilely on a coordinate measuring machine (CMM) in an air-conditioned measuring room. On the coordinate measuring machine type

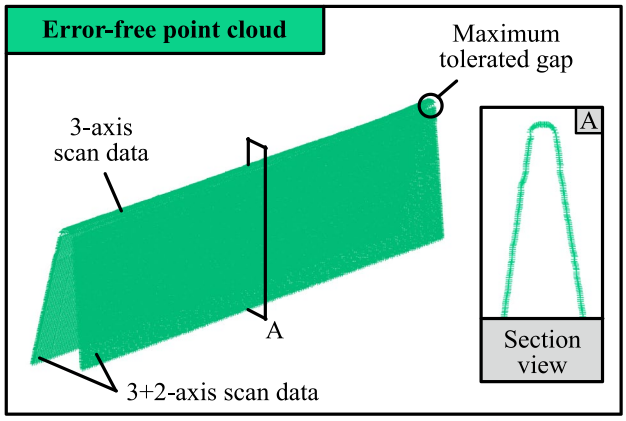

Fig. 14 Error-free point cloud of leading edge

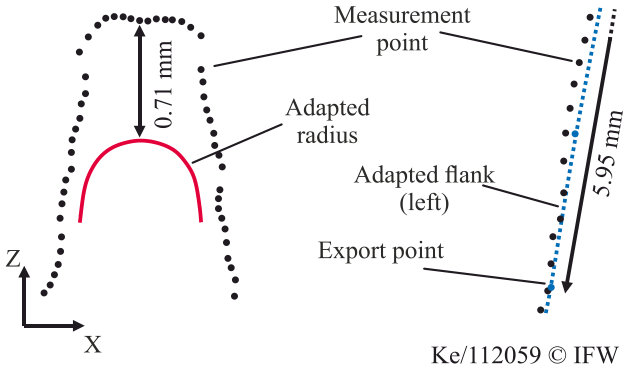

Fig. 15 Evaluation of the adaption at cutting position at 88% of the length

Leitz Reference XI 10 7 6/B5, 10 differently defined sections, which also had a scanned measuring line, were measured with a 3 mm measuring sphere. Thus, it was possible to make a direct comparison. The radius correction of the tactile probe was achieved with Hexagon's Quindos software using the Crv2DMorphRadCor method, point distance of 0.04 mm. Because the generated point distance in the section varied between both measuring methods, the smallest distances were determined by a self-developed algorithm. An average deviation of approx. 40 µm between the scanned and tactilely measured points was determined. These deviations include clamping, alignment, axis and compensation errors, etc. In the direct visual comparison of both point clouds, a slight tilt and minimal offset were visible. This can be explained by a different mounting, alignment of the measurement plane, and deviations of the reference zero point. To sum up, the determined deviation is minor including the errors mentioned and the scanning system is very well suited for this difficult application.

In addition, the set-up and measurement speed of both methods were compared. For the set-up on the CMM, consisting of clamping, adjusting, zeroing, and measuring path programming, a time of approximately 60 min was required. The tactile measurement of one section took about 20 s. Furthermore, after the tactile measurement, a subsequent compensation of the probe radius in the recorded measurement data was necessary, which also requires time and technical expertise. For the presented fully automated scanning method, an oriented scanning system in the CNC machine tool is essential. With the help of a calibration sample, the laser line sensor can be aligned in the workpiece coordinate system within 5–10 min. The automated probing (zero-point set) and scanning of the part (1×3 axis and $2 \times 3 + 2$ axis scan) took 10 min according to the set feed rate of 50 mm/min and reduced rapid traverse speed to 20%. A total of 220 scan lines (sections) per surface / per part were saved. The automated filtering of the recorded data, with the presented algorithm, was done in seconds. Thus, by using the scanning system instead of a tactile measurement on the coordinate measuring machine, 1/7 of the initial measurement time was needed. In summary, the following advantages can be achieved by using the scanning method for leading edges:

(1) high measuring speed,
(2) less set-up time and path planning effort,
(3) no re-clamping of the sample.
(4) no clamping deviation,
(5) simplified data processing,
(6) transport routes and planning are not necessary, and.
(7) no expensive measuring machine is required.

Using the acquired point cloud of the worn model, the initial CAD-model of the new workpiece was adapted by the method presented in Sect. 3 to obtain an optimized target model. The rigid transformation was conducted twenty times until a sufficient alignment could be ensured. The transition distance was 6 mm and no additional pole points were added. The resulting intersection curves were used to reconstruct the surface. The material removed from the top was about 0.7 to 1.3 mm, depending on the measurement position. As shown in Fig. 15, the radius was well-fitted in the X-direction. The flank approaches the point cloud near the 6 mm mark. Using the reconstructed surface, an automated process planning was conducted.

For the re-contouring, a SECO solid carbide ball end mill, with a diameter of 8 mm and six cutting edges, was used (JS730080D2B.0Z6-HXT). The machine tool used for scanning was not able to properly process the material Ti6Al4V due to the deactivated cooling lubricant system from the integration of strain gauges [33]. However, as the Ti6Al4V material is commonly used in the aerospace industry, the first re-contouring experiments were performed on the DMG MORI DMU 125P CNC machine tool with this material.

Results show severe deviations due to the transfer between the machines and the necessary recalibration. A zero-point (clamping) system was not suitable for the transfer as this process focuses on a flexible approach for re-contouring many different types and sizes of blades. For this, many different zero-point systems would be necessary. In order to show the capability of the overall process, the material was changed to the highly alloyed steel X8CrNiS18-9, which can be processed dry on the CNC-machine tool DMG HSC 55 linear used for scanning.

To achieve a high level of shape accuracy, the HSC 55 machine axes were calibrated before the experimental validation of the presented process chain began. This was done with a calibration cycle DMG MORI 3D Quickset based on tool data measured with a pre-setter Zoller Venturion 450. For the re-contouring process, a feed rate of 2005 mm/min and a spindle speed of 4178 rpm was used. The re-contouring result is shown in Fig. 16. As shown in the picture, the leading edge and both of the side areas were equally processed. In detail, the resulting radius at the tip was manufactured adequately. For example, a manually fitted radius at the cutting plane of 12 mm is about 0.68 mm, while the radius of the initial CAD-model is 0.66 mm. This is shown in Fig. 17.

The achieved radius shows small shape deviations. The maximum deviation is 0.031 mm at the tip of the workpiece. Both shape and dimensional accuracy are very promising and, if transferred to a real blade, should result in a good overall performance. Additionally, the continuous transition between the machined and unmachined parts of the workpiece is as smooth as planned. Due to the discrete measurement of the surface (CMM, radius correction: Crv2DMorphRadCor), the tangentiality cannot be quantified. Optical inspection of experts, as well as manual touching (fingernail scratch test), confirm the initial visual impression.

As the idea to generate a smooth transition between the machined and unmachined parts only by milling was

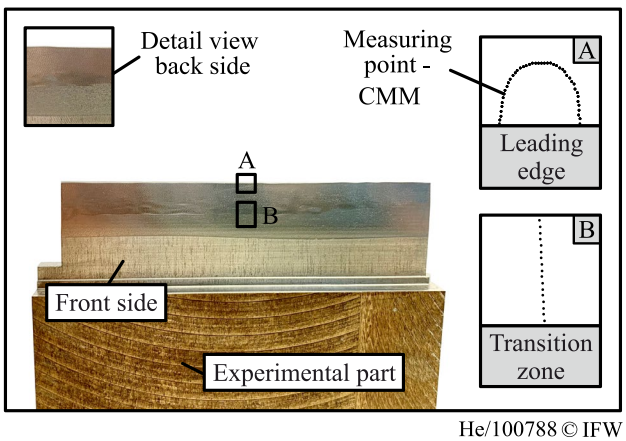

He/100788 © IFW

Fig. 16 Result of the re-contouring a leading edge-experimental part

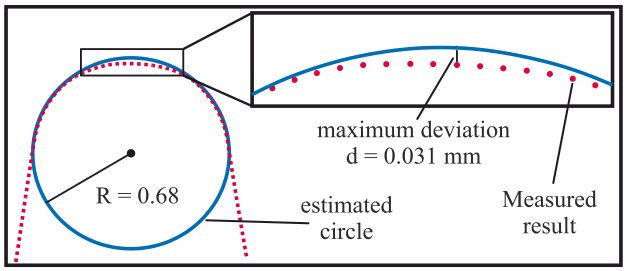

Ke/112060 © IFW

Fig. 17 Manufactured radius at cutting plane of 12 mm and shape deviation

accomplished, industrialization of the process is possible. In industry state-of-the-art, additional manufacturing processes, like vibratory grinding or barrel finishing, are conducted afterward. In this process, the material removal is very small but very likely sufficient for the elimination of all the optical traces of the transition line. In combination with the achieved geometric accuracy of the leading edge radius, the overall results are promising.

5 Discussion

As explained in the previous section, the experimental results are very promising but highly dependent upon the machine and measuring accuracy. While minor deviations in the radius part of the leading edge are not an issue for the re-contouring, small deviations in the transition between the machined and unmachined parts can result in sharp edges on the surface. This results in an unsmooth surface which has a big influence on the performance of the blade. As almost all measuring systems record discrete points, the shape between the measuring points can only be estimated. The smaller the edge to be measured, the fewer the measuring points that exist to describe the edge. This results in an inevitable inaccuracy. Additionally, three main challenges that might influence the smooth transition were identified. Firstly, the point cloud of the surface has a scanning-process-dependent uncertainty. Thus, the planned shape is adapted to uncertain and noise-afflicted points. Secondly, during the manufacturing of these areas, the machine axes are in extreme positions in comparison to the positions of the axes during the scan. Therefore, the uncertainties of the axes-positions are added up for the relative position between the planned position on the scanned surface and the actual position of the tool. Even though the position uncertainty of the machine axes on a well-calibrated CNC machine tool is very small, the maximum axes' deflection and the extreme tolerance requirements of the smooth transition process may cause visible edges on the surface. Thirdly, the cutting volume

decreases in the area of the transition between the machined and unmachined surface until it is zero at the point of transition. Thus, the chip thickness falls below the tool-specific minimum value. To minimize inaccuracy and deviations, it was determined that the measurement and re-contouring on the same machine is of the utmost importance. When changing the machine, another source of deviation is added by calibrating the workpiece in the machine coordinate system.

While the experimental results are good, some additional processes might improve the results, especially in an industrial process. To improve the re-contouring process itself, displacement modeling and tool path adaption, which is part of several current and completed research projects, should be included in the presented process. Additionally, the integration of the process in a digital twin approach might be beneficial for tasks like predictive maintenance and overall acceleration of the engine repair process. In future work, the process needs to be adapted to real blade types and evaluated in an industrial environment. In addition, the use of a CFD simulation to benchmark the re-contouring result and optimize the steps of the process chain would also be thinkable. To gain more knowledge about the process and its limitations, scientific studies need to be conducted with real blades at an MRO service provider. With these steps, industrial implementation of the presented method can be accomplished.

In conclusion, the presented process is a new and innovative method for the re-contouring of blades. While other, similar methods mainly focus on the re-contouring of weld-cladded blades, this process tries to extend the lifespan of the blade without energy- and time-consuming material addition processes. Thus, the presented method can be seen as a link between a new part production and the unavoidable welding repair. Given the looming climate catastrophe, this is an important partial step towards more sustainable engine repair. Additionally, the direct re-contouring approach in the presented process chain is much faster than the welding repair. Furthermore, the presented method is highly automated, which makes the re-contouring repeatable and easy to use, particularly with regard to the acute shortage of skilled workers.

6 Conclusion and outlook

In this paper, a process for the re-contouring of leading edges in aircraft engines was presented. The process consists of a scanning process to acquire the actual contour of the worn blade, an adaption process to generate a target model based on the initial CAD-model, and an automated process planning. The method was researched using a workpiece that represents common blade types. It could be shown that an integrated approach for the repair of worn blades is suitable for achieving a geometric reconstruction of the radius. A smooth transition between the machined and unmachined parts of the workpiece could be realized using only milling operations. State-of-the-art methods for smoothing, which are conducted anyway, are expected to smoothen the surface even more. To improve the process chain, the accuracy of the shape acquisition needs to be enhanced for small parts with high curvature, as presented in the area of the radius. Furthermore, the adaption process needs to be more flexible between single profiles. Currently, the adaption completely follows the existing point cloud, which leads to waves along the length of the workpiece. In order to compensate for noise and prevent these waves, the deviation between intersection profiles must be limited and smoothened. Finally, a new process planning for the removal of very small volumes of material needs to be implemented to achieve the goal of a milling-based smooth transition between the machined and the unmachined parts.

Acknowledgements The authors thank the German Research Foundation (DFG) for the financial support within the transfer project "Automated re-contouring of fan blades" of the Collaborative Research Center 871: Regeneration of complex capital goods. Further thanks are extended to the Lower Saxony Ministry for Science and Culture (MWK) for funding the MOBILISE - PL5 "Regeneration of Moulding Tools for Mass-Suitable Lightweight Design". In addition, the authors thank the Sieglinde Vollmer Foundation for supporting this research.

Funding Open Access funding enabled and organized by Projekt DEAL. This work was funded by Deutsche Forschungsgemeinschaft, 119193472 and Niedersächsische Ministerium für Wissenschaft und Kultur, Mobilise PL-5.

Data availability The experimental data are not available due to commercial reasons.

Declarations

Conflict of interest The authors declare that they have no conflict of interest.

References

1. Pratt & Whitney – An RTX Business (2014) V2500 engine cutaway. https://prd-sc102-cdn.rtx.com/-/media/pw/products/comme

rcial-jet-engines/v2500/files/v2500-engine-cutaway.jpg. Accessed 12 Jan 2024
2. Saha PK (2016) Aerospace Manufacturing processes. CRC Press, Boca Raton, London, New York. https://doi.org/10.1201/9781315367965
3. AIRBUS SAS (2021) Airbus Global Market Forecast 2021–2040
4. Statista Projected global engine MRO demand from 2021 to 2030, by type (in billion U.S. dollars) [Graph], release date February 3, 2021, (Retrieved December 14, 2021). https://www.statista.com/statistics/1201134/projected-global-engine-mro-demand-type/
5. The Federal Aviation Administration (FAA) (2021) Flight Standards Information Management System (FSIMS), Volume 3 General Technical Administration, Chap. 15 Foundational Information, Sect. 1 The Elements of Maintenance, 3-592
6. Rossmann A (2000) Die Sicherheit Von Turbo-Flugtriebwerken, vol 1—2. Turbo Consult, Karlsfeld
7. Vogel H, Kando A, Schulte H, Staudacher S (2018) A Top-Down Approach for quantifying the contribution of high pressure compressor deterioration mechanisms to the performance deterioration of Turbofan engines. In: Proceeding of ASME Turbo Expo 2018 Turbomach Tech Conf Exposition GT2018 Oslo nor, pp 1–10. https://doi.org/10.1115/GT2018-75558
8. Roberts WB, Armin A, Kassaseya G, Suder KL, Throp SA, Strazisar AJ (2002) The effect of variable chord length on Transonic Axial Rotor Performance, transactions of the ASME. J Turbomach 124(3):351–357. https://doi.org/10.1115/1.1459734
9. Czerner S (2012) Method for recontouring a compressor blade or a turbine blade for a gas turbine, Patent. US2012047735A1
10. Czerner S (2015) Device for re-contouring a gas turbine blade, Patent. US9040870B2
11. Peters JO, Gartner TD, Schön J, Kuntzagk S (2021) Device and method for re-contouring a gas turbine blade, Patent. US11141800B2
12. Subbiah S, Mande A (2012) An apparatus and a method of shaping an edge of an airfoil. Patent EP 2 530(242):A2
13. Giebmanns AG, Schnell R, Steinert W, Hergt A, Nicke E, Werner-Spatz C (2012) Analyzing and optimizing geometrically degraded Transonic Fan blades by means of 2D and 3D simulations and Cascade measurements. In: Proceeding of ASME Turbo Expo 2012 GT2012 Cph Denmark, pp 279–288. https://doi.org/10.1115/GT2012-69064
14. Larsson J, Elofsson A, Sterner T, Åkerman J (2019) International and national climate policies for aviation: a review. Clim Policy 19(6):787–799. https://doi.org/10.1080/14693062.2018.1562871
15. Uhlmann E, Bilz M, Baumgarten J (2013) MRO – challenge and chance for sustainable enterprises. Procedia CIRP 11:239–244. https://doi.org/10.1016/j.procir.2013.07.036
16. Denkena B, Boess V, Nespor D, Floeter F, Rust F (2015) Engine blade regeneration: a literature review on common technologies in terms of machining. Int J Adv Manuf Technol 81:917–924. https://doi.org/10.1007/s00170-015-7256-2
17. Bremer C (2005) Automated Repair and overhaul of aero-engine and industrial gas turbine components. In: Proceedings of GT2005, ASME Turbo Expo 2005: Power for land, sea, and air, Reno-Tahoe, Nevada, USA, pp 841–846. https://doi.org/10.1115/GT2005-68193
18. Thorenz B (2021) Entwicklung eines Schafteckfräsers mit Leichtbau-Innenkern zur schwingungsreduzierten Fräsbearbeitung. Dr.-Ing. Thesis, Bayreuthn
19. Klocke F (2011) Manufacturing processes 1, cutting. Springer, Berlin Heidelberg
20. Gey C (2002) Prozessauslegung für das Flankenfräsen von Titan, Dr.-Ing. Thesis, Hannover
21. Meinecke M (2009) Prozessauslegung zum fünfachsigen zirkularen Schruppfräsen von Titanlegierungen, Dr.-Ing. Thesis, Aachen
22. Gao J, Chen X, Yilmaz O, Gindy N (2008) An integrated adaptive repair solution for complex aerospace components through geometry reconstruction. Int J Adv Manuf Technol 36:1170–1179. https://doi.org/10.1007/s00170-006-0923-6
23. Wu B, Zheng H, Wang J, Zhang Y (2020) Geometric model reconstruction and CNC machining for damaged blade repair. Int J Comput Integr Manuf 33(3):287–301. https://doi.org/10.1080/0951192X.2020.1736710
24. Zheng-Qing Z, Yun Z, Zhi-Tong C (2020) A repair strategy based on tool path modification for damaged turbine blade. Int J Adv Manuf Technol 106:2995–3006. https://doi.org/10.1007/s00170-019-04801-z
25. Cui K, Jiang R-S, Jing L (2022) Model reconstruction for worn blades based on hybrid surface registrations. Adv Manuf 10:479–494. https://doi.org/10.1007/s40436-022-00390-5
26. Ünal-Saewe T, Gahn L, Kittel J, Gasser A, Schleifenbaum JH (2020) Process development for tip repair of complex shaped turbine blades with IN718. 47:1050–1057. 10.1016/j.promfg.2020.04.114.
27. Yu H, Lyu X (2018) Repair of defective 3D blade model based on deformation of adjacent non-defective cross-sectional curve. Int J Adv Manuf Technol 95:3045–3055. https://doi.org/10.1007/s00170-017-1393-8
28. Yan C, Wan W, Huang K, Liu L, Lee C-H (2020) A reconstruction strategy based on CSC registration for turbine blades repairing. Robot Comput Integr Manuf 61:101835. https://doi.org/10.1016/j.rcim.2019.101835
29. Huang Z, Wei P, Li C, Wang H, Wang J (2020) Aero-engine blade profile reconstruction based on adaptive step size bat algorithm and visualization of machining error. Proc Inst Mech Eng Part C 234(1):49–65. https://doi.org/10.1177/0954406219874840
30. Yu H, Lyu X, Liu P (2019) Stream surface reconstruction of aero engine blade based on limited measured points. Adv Eng Softw 131:90–101. https://doi.org/10.1016/j.advengsoft.2019.02.008
31. Keyence, Corporation (2022) Data sheet LJ-V7080 sensor head
32. Denkena B, Böß V, Dittrich M-A, Kenneweg R (2020) Function-optimised generation of an adapted target model for mechanical re-contouring of fan blades. In: 53rd CIRP Conference on Manufacturing Systems, Procedia CIRP 93, pp 562–567. https://doi.org/10.1016/j.procir.2020.05.161
33. Denkena B, Boujnah H (2018) Feeling machines for online detection and compensation of tool deflection in milling. CIRP Ann 67(1):423–426. https://doi.org/10.1016/j.cirp.2018.04.110